Exact diagonalization study of the effects of Zn and Ni impurities on the pseudogap of underdoped cuprate high-T_c superconductors

Jiří Vašátko[1] and Dominik Munzar[1,2]

[1]*Department of Condensed Matter Physics, Faculty of Science, Masaryk University, Kotlářská 2, 61137 Brno, Czech Republic*

[2]*Central European Institute of Technology, Masaryk University, Kamenice 753/5, 62500 Brno, Czech Republic*

(Received 14 December 2015; published 9 March 2016)

The influence of Zn and Ni impurities on the normal-state pseudogap of underdoped high-T_c cuprate superconductors is studied using exact diagonalization of effective t-J-like Hamiltonians describing low energy electronic excitations of the CuO_2 plane with some of the copper ions replaced with Zn/Ni. The Ni case Hamiltonian has been obtained by a sequence of approximations from a more complete model involving Cu $3d$, Ni $3d$, and O $2p$ orbitals. Our main findings are: (i) The width Ω_{PG} of the pseudogap occurring in the many body density of states, and manifesting itself also in the c-axis infrared conductivity, decreases with increasing Zn concentration as a consequence of a suppression of short range spin correlations. (ii) In the case of one hole and one Ni impurity, the hole is—for realistic values of the model parameters—weakly bound to the Ni site. This causes a slight increase of Ω_{PG} with respect to the pure case. (iii) Based on this result and further results for 1–2 holes and 1–2 Ni impurities, we suggest that in the real Ni substituted CuO_2 plane Ω_{PG} is larger than in the pure case due to the binding of the doped holes to the Ni sites and effective underdoping. Our findings clarify the trends observed in the c-axis infrared conductivity data of Zn and Ni substituted (Sm,Nd)$Ba_2Cu_3O_{7-\delta}$ crystals.

DOI: 10.1103/PhysRevB.93.094512

I. INTRODUCTION

The origin of the pseudogap of underdoped cuprate superconductors, consisting in a partial gaplike suppression of the densities of low-energy spin and charge excitations, occurring in the temperature range from the superconducting transition temperature T_c to the onset temperature T^* [1–6], ranks among the major unsolved problems in the field of high-T_c superconductivity [7–10]. In particular, it is debated, what is the order/broken symmetry associated with the pseudogap (if any) and what is the relation between the pseudogap and superconductivity. The first spectroscopic evidence for a pseudogap in a high-T_c superconductor came in 1993 when Homes and co-workers demonstrated that the real part $\sigma_{1c}(\omega)$ of the c-axis infrared conductivity $\sigma_c(\omega)$ of underdoped $YBa_2Cu_3O_{6.6}$ exhibits a gaplike depression persisting up to room temperature [3,11]. Subsequent studies of σ_c revealed many important aspects of the pseudogap, among others the following. (i) The pseudogap in σ_{1c} is simply connected to the one observed by photoemission [12]. (ii) The dependence of the pseudogap energy scale (width) Ω_{PG} on the hole concentration δ can be approximated by a linear function crossing the horizontal axis around 0.20 and the vertical axis around 250 meV [13]. (iii) The transfers of the optical spectral weight associated with the pseudogap setting on at T^* are not compatible with the hypothesis that it is due to superconducting pairing without long range phase coherence [13]. Pairing correlations seem to set on at a temperature T^{ons} significantly higher than T_c but at the same time substantially lower than T^* [14,15]. (iv) The pseudogap is vulnerable to the presence of Zn impurities [16]. In contrast, Ni impurities cause a strong enhancement of the pseudogap [16]. While the finding (iv) has been suggested to imply a prominent role of magnetic correlations, this idea has not yet—to the best of our knowledge—been supported by any quantitative considerations.

Here we report on results of our calculations of the many body density of states $N(\omega)$ and of $\sigma_{1c}(\omega)$ for models representing the CuO_2 plane, where some of the Cu ions are replaced with Zn/Ni ions. These results clarify most of the impurity related trends reported in Ref. [16], in particular, the Zn(Ni) induced decrease (increase) of Ω_{PG}. For reference calculations of the electronic properties of the pure CuO_2 plane, we use the t-J Hamiltonian [17]. It has been shown early on by Prelovšek and co-workers [18–20] that this standard Hamiltonian gives rise to a pseudogap in $N(\omega)$ and $\sigma_{1c}(\omega)$. Note that Ω_{PG} of this pseudogap is—for low values of δ and in the absence of impurities—approximately equal to $2J$, and that a relatively recent advanced study of the Hubbard model at intermediate coupling provides a comparable pseudogap [21]. Our aim has been to find out how the pseudogap is influenced by the presence of Zn/Ni. For calculations of the Zn substituted case, we have used the corresponding modification of the t-J Hamiltonian devised by Poilblanc, Scalapino, and Hanke [22]. For calculations of the Ni substituted case, we use an effective t-J-like Hamiltonian, that we have obtained by a sequence of approximations from the Hubbard-type Hamiltonian proposed, as a starting point for analyzing the effects of Ni impurities, by Tsutsui and co-workers [23] and further used by Ishii and co-workers [24].

The rest of the paper is organized as follows. In Sec. II we present the effective Hamiltonians, the one used in the Ni substituted case is derived starting from the Hubbard-type Hamiltonian of Ref. [23]. In Sec. III we present and discuss our results. In Sec. III A we focus on the many body density of states, address the origin of the t-J model pseudogap, and the Zn- and Ni-induced changes of its magnitude. In Sec. III B we address the calculated conductivity spectra and compare them with the experimental data of Ref. [16]. A summary and conclusions are given in Sec. IV.

II. EFFECTIVE HAMILTONIANS FOR Ni AND Zn SUBSTITUTED CUPRATES

Zhang and Rice derived a single band effective t-J Hamiltonian for the doped CuO_2 plane starting from the two band Hubbard model [25]. The underlying assumption is that doped holes reside in the so called Zhang-Rice singlets. A singlet involves a hole on a Cu site and a doped hole in a symmetry adapted molecular orbital of the neighboring oxygen sites. In the first part of this section we derive, following their approach, an effective low energy t-J-like model for the CuO_2 plane, where some of the Cu ions are replaced with Ni ions. As a starting point we use the Hubbard-type Hamiltonian proposed by Tsutsui *et al.* [23]: $H = H_T + H_d$ with

$$\begin{aligned} H_T =& T_{pd}\sum_{\mathbf{i}\sigma} d^{\dagger}_{\mathbf{i}\sigma}\left(p_{\mathbf{i}-\frac{\mathbf{x}}{2}\sigma} - p_{\mathbf{i}+\frac{\mathbf{x}}{2}\sigma} - p_{\mathbf{i}-\frac{\mathbf{y}}{2}\sigma} + p_{\mathbf{i}+\frac{\mathbf{y}}{2}\sigma}\right) \\ &- T'_{pd}\sum_{\mathbf{i_0}\sigma} d'^{\dagger}_{\mathbf{i_0}\sigma}\left(p_{\mathbf{i_0}-\frac{\mathbf{x}}{2}\sigma} - p_{\mathbf{i_0}+\frac{\mathbf{x}}{2}\sigma} + p_{\mathbf{i_0}-\frac{\mathbf{y}}{2}\sigma} - p_{\mathbf{i_0}+\frac{\mathbf{y}}{2}\sigma}\right) \\ &+ \alpha T''_{pd}\sum_{\mathbf{i_0}\sigma} d'^{\dagger}_{\mathbf{i_0}\sigma}(p_{\mathbf{i_0}-\mathbf{z}\sigma} - p_{\mathbf{i_0}+\mathbf{z}\sigma}) + \text{ H.c.} \\ &+ \epsilon_d\sum_{\mathbf{i}\neq\mathbf{i_0}\sigma} n^d_{\mathbf{i}\sigma} + \epsilon_{\mathrm{Ni}}\sum_{\mathbf{i_0}\sigma\gamma=d,d'} n^{\gamma}_{\mathbf{i_0}\sigma} + \epsilon_p\sum_{\mathbf{i}\delta\sigma} n^p_{\mathbf{i}+\frac{\delta}{2}} \end{aligned} \tag{1}$$

and

$$\begin{aligned} H_d =& U_d\sum_{\mathbf{i}\neq\mathbf{i_0}} n^d_{\mathbf{i}\uparrow}n^d_{\mathbf{i}\downarrow} + U_{\mathrm{Ni}}\sum_{\mathbf{i_0}\gamma} n^{\gamma}_{\mathbf{i_0}\uparrow}n^{\gamma}_{\mathbf{i_0}\downarrow} + U'_{\mathrm{Ni}}\sum_{\mathbf{i_0}\sigma\sigma'} n^d_{\mathbf{i_0}\sigma}n^{d'}_{\mathbf{i_0}\sigma'} \\ &+ K_{\mathrm{Ni}}\sum_{\mathbf{i_0}\sigma\sigma'} d^{\dagger}_{\mathbf{i_0}\sigma}d'^{\dagger}_{\mathbf{i_0}\sigma'}d_{\mathbf{i_0}\sigma'}d'_{\mathbf{i_0}\sigma} \\ &+ K_{\mathrm{Ni}}\sum_{\mathbf{i_0}}(d^{\dagger}_{\mathbf{i_0}\uparrow}d^{\dagger}_{\mathbf{i_0}\downarrow}d'_{\mathbf{i_0}\downarrow}d'_{\mathbf{i_0}\uparrow} + \text{H.c.}). \end{aligned} \tag{2}$$

It is given in the hole representation and it involves Cu and Ni $3d_{x^2-y^2}$ orbitals (operators d, $d^{\dagger}$), planar oxygen $2p_x$ and $2p_y$ orbitals (p, $p^{\dagger}$), Ni $3d_{3z^2-r^2}$ orbitals (d', $d'^{\dagger}$), and p_z orbitals of the apical oxygens located above or below the Ni ions (p_z, $p_z^{\dagger}$). The summation over $\mathbf{i}$ runs over all Cu and Ni sites, $\mathbf{i_0}$ denotes Ni sites. For the meaning of the other symbols, see Ref. [23]. The interaction terms for a Ni site in Eq. (2) correspond to the multiorbital Hubbard model introduced by Oleś [26]. The fourth term can be written as

$$-2K_{\mathrm{Ni}}\sum_{\mathbf{i_0}}\left(\mathbf{S}'_{\mathbf{i_0}}\mathbf{S}_{\mathbf{i_0}} + \frac{1}{4}n_{\mathbf{i_0}}n'_{\mathbf{i_0}}\right), \tag{3}$$

where $\mathbf{S}_{\mathbf{i_0}}$ and $\mathbf{S}'_{\mathbf{i_0}}$ are the spin operators of the d orbital and of the d' orbital, respectively, and $n_{\mathbf{i_0}}$ and $n'_{\mathbf{i_0}}$ are the corresponding hole number operators.

Tsutsui *et al.* further expressed H_T in terms of symmetric ($\phi^s_{\mathbf{i}}$) and antisymmetric ($\phi^a_{\mathbf{i}}$) oxygen Wannier orbitals:

$$\begin{aligned} H_T =& 2T_{pd}\sum_{\mathbf{ij}\sigma}\left(\tau_{\mathbf{ij}}d^{\dagger}_{\mathbf{i}\sigma}\phi^s_{\mathbf{j}\sigma} + \text{H.c.}\right) \\ &- 2T'_{pd}\sum_{\mathbf{i_0j}\sigma}\left(\tau'^{s}_{\mathbf{i_0j}}d'^{\dagger}_{\mathbf{i_0}\sigma}\phi^s_{\mathbf{j}\sigma} + \text{H.c.}\right) \\ &+ 2\sqrt{2}T'_{pd}\sum_{\mathbf{i_0j}\sigma}\left(\tau'^{a}_{\mathbf{i_0j}}d'^{\dagger}_{\mathbf{i_0}\sigma}\phi^a_{\mathbf{j}\sigma} + \text{H.c.}\right) \\ &+ \epsilon_p\sum_{\mathbf{i}\sigma\eta=s,a}\phi^{\eta+}_{\mathbf{i}\sigma}\phi^{\eta}_{\mathbf{i}\sigma} + \epsilon_{\mathrm{Ni}}\sum_{\mathbf{i_0}\sigma\gamma=d,d'} n^{\gamma}_{\mathbf{i_0}\sigma}, \end{aligned} \tag{4}$$

with

$$\begin{aligned} \phi^a_{\mathbf{i}\sigma} =& -iN^{-\frac{1}{2}}\sum_{\mathbf{k}} e^{i\mathbf{ki}}\beta_{a\mathbf{k}}\left[\sqrt{2}s_x s_y(s_y p_{x\mathbf{k}\sigma} + s_y p_{y\mathbf{k}\sigma})\right. \\ &\left. - i\alpha\left(s_x^2 + s_y^2\right)p_{z\mathbf{k}\sigma}\right], \\ \phi^s_{\mathbf{i}\sigma} =& -iN^{-\frac{1}{2}}\sum_{\mathbf{k}} e^{i\mathbf{ki}}\beta_{\mathbf{k}}(s_x p_{x\mathbf{k}\sigma} - s_y p_{y\mathbf{k}\sigma}), \end{aligned} \tag{5}$$

where

$$\begin{aligned} &\beta_{\mathbf{k}} = \left(s_x^2 + s_y^2\right)^{-1/2}, \quad \beta_{a\mathbf{k}} = \beta_{\mathbf{k}}\left(2s_x^2 s_y^2 + \alpha^2\beta_{\mathbf{k}}^{-2}\right)^{-1/2}, \\ &s_{x(y)} = \sin\frac{k_{x(y)}}{2}, \\ &\tau_{\mathbf{ij}} = \frac{1}{N}\sum_{\mathbf{k}}\beta_{\mathbf{k}}^{-1}e^{i\mathbf{k}(\mathbf{i}-\mathbf{j})}, \\ &\tau'^{s}_{\mathbf{ij}} = \frac{1}{N}\sum_{\mathbf{k}}\beta_{\mathbf{k}}\left(s_x^2 - s_y^2\right)e^{i\mathbf{k}(\mathbf{i}-\mathbf{j})}, \\ &\tau'^{a}_{\mathbf{ij}} = \frac{1}{N}\sum_{\mathbf{k}}\beta_{\mathbf{k}}^2\beta_{a\mathbf{k}}^{-1}e^{i\mathbf{k}(\mathbf{i}-\mathbf{j})}. \end{aligned} \tag{6}$$

The parameter ϵ_d has been set equal to zero. The values of the coefficients $\tau_{\mathbf{ij}}$, $\tau'^{s}_{\mathbf{ij}}$, $\tau'^{a}_{\mathbf{ij}}$ drop fast with increasing distance between the sites $\mathbf{i}$ and $\mathbf{j}$. The charge transfer energy of the Ni sites (i.e., the energy difference between the two-hole states $d^9\underline{L}$ and d^8) will be labeled as Δ_{Ni}, $\Delta_{\mathrm{Ni}} = \epsilon_p - \epsilon_{\mathrm{Ni}} - U_{\mathrm{Ni}} + 3K_{\mathrm{Ni}}$, and the difference between Δ_{Ni} and the charge transfer energy of the Cu sites ϵ_p as $\tilde{\Delta}$, $\tilde{\Delta} = \Delta_{\mathrm{Ni}} - \epsilon_p$.

In the absence of doped holes, the ground state of the Hamiltonian involves one hole per Cu ion and two holes per Ni ion. The two holes in the Ni d and d' orbitals prefer to form a triplet, the energy difference between the triplet and the singlet being $-2K_{\mathrm{Ni}}$. Upon hole doping, the additional holes can occupy oxygen orbitals surrounding Cu sites, forming the Zhang-Rice singlets as in the case of the pure CuO_2 plane. But Tsutsui *et al.* [23] demonstrated that for values of $\tilde{\Delta}$ above a critical value of $\sim$1.2 eV, the holes occupy mainly the oxygen orbitals surrounding the Ni sites, forming Zhang-Rice doublets.

Before proceeding along the lines of Zhang and Rice, the Hamiltonian given by Eqs. (2) and (4) has to be further simplified. In the following, the necessary simplifications will be motivated by results of exact diagonalization of the original Hamiltonian for small clusters. In all Hubbard model based calculations, we have used the same values of the input parameters as in Ref. [23]: $T_{pd} = 1$ eV, $T'_{pd} = T_{pd}/\sqrt{3}$, $T''_{pd} = 2T_{pd}/\sqrt{3}$, $U_d = U_{\mathrm{Ni}} = 8$ eV, $K_{\mathrm{Ni}} = 0.8$ eV, $\epsilon_p = 3$ eV, $\alpha = 1/\sqrt{2}$. Several values of the remaining parameter ϵ_{Ni} (or $\tilde{\Delta}$) have been used, they are specified where appropriate.

In Table I we present results of exact diagonalization for a cluster containing one Ni site with its d and d' orbitals and with the corresponding oxygen Wannier orbitals ϕ^s and ϕ^a. The upper (bottom) part corresponds to the undoped (doped) case with two (three) holes in total. It can be seen in the upper part that the ground state of the undoped case is a triplet, with major contributions of the dd' triplet states. The triplet is reasonably separated from excited states. It can be seen in the bottom part that the ground state of the doped case is a doublet. Its spin up (spin down) component can be expressed as $0.68|d'_\uparrow\rangle(|\phi^s_\uparrow d_\downarrow\rangle - |\phi^s_\downarrow d_\uparrow\rangle)/\sqrt{2}$ + smaller terms $[0.68|d'_\downarrow\rangle(|\phi^s_\downarrow d_\uparrow\rangle - |\phi^s_\uparrow d_\downarrow\rangle)/\sqrt{2}$ + smaller terms]. The components will be denoted as components of the Zhang-Rice (ZR) doublet in the following. The ZR doublet is followed by another doublet, whose components can be similarly approximated as products of the $\phi^a d'$ singlet and the d spin down state/d spin up state. They will be denoted as components of the A doublet. The distance in energy between the ZR doublet and the A doublet is only 0.37 eV and it appears that the effective low-energy Hamiltonian should thus perhaps include both. Fortunately, the distance increases with increasing size of the cluster as illustrated in Table II. The table shows the lowest energy eigenvalues and the corresponding averaged hole numbers (n) per orbitals for the doped single Ni cluster discussed above and for a doped four-site cluster containing three Cu ions and one Ni ion, together with the neighboring oxygens, subject to the periodic boundary conditions. It can be seen that for the larger cluster, the energy of the lowest eigenstate with $n(\phi^a) > n(\phi^s_0)$ (-11.42 eV) is by more than 0.7 eV higher than that of the ground state, much more than for the single Ni cluster. The trend can be understood as follows: The coupling between ϕ^a and Ni d' leading to the formation of the A doublet, described by the third term on the right-hand side of Eq. (4), is strong on site, but it diminishes fast with increasing distance from the impurity. For systems with low Ni concentration, where the Ni ions are separated by Cu ions, the A doublets are therefore fairly localized. The ZR doublets, on the other hand, hybridize with the ZR singlets of the Cu sites. A state involving the ZR doublet at a Ni site and the one-hole configuration at a neighboring Cu site can transform into the state involving the triplet at the Ni site and the ZR singlet at the Cu site and vice versa [27]. This provides a lowering of the in-plane kinetic energy of the ZR doublet states with respect to the A doublet ones.

Motivated by these observations, we limit ourselves to the Hilbert space spanned by states involving the following configurations of the Ni sites: dd' (both the triplet states and the singlet states, only the former, however, are relevant at low energies), and the two components of the ZR doublet. This reduction is justified by results shown in Table I and by $n(\mathrm{Ni}\,d) \approx 1$ and $n(\mathrm{Ni}\,d') \approx 1$ in Table II. Concerning the Cu sites, only the one hole and the ZR singlet configurations have been allowed, as in the Zhang-Rice paper.

Next we address the roles of the components of the Hamiltonian of Eqs. (2) and (4). The first, the second, and the third terms on the right-hand side of Eq. (2) are used in perturbation expansions only. In the fourth term, given by Eq. (3), we have neglected the almost constant products $n_{\mathbf{i}_0} n'_{\mathbf{i}_0}$. The contributions of this term to the energies of the

TABLE I. Results of exact diagonalization for a cluster containing a single Ni ion and the on-site Wannier oxygen orbitals. The value of the parameter $\tilde{\Delta}$ is set equal to 1.4 eV. The upper (bottom) part corresponds to the undoped (doped) case with two (three) holes in total.

E (eV)	Two-hole eigenstate
−9.551860	$0.9\lvert d'_\uparrow d_\uparrow\rangle + 0.33\lvert\phi^s_\uparrow d'_\downarrow\rangle - 0.27\lvert\phi^a_\uparrow d_\uparrow\rangle + 0.065\lvert\phi^a_\uparrow\phi^s_\uparrow\rangle$
−9.551860	$0.9(\lvert d'_\uparrow d_\downarrow\rangle + \lvert d'_\downarrow d_\uparrow\rangle)/\sqrt{2} + 0.33(\lvert\phi^s_\downarrow d'_\uparrow\rangle + \lvert\phi^s_\uparrow d'_\downarrow\rangle)/\sqrt{2} - 0.27(\lvert\phi^a_\downarrow d_\uparrow\rangle + \lvert\phi^a_\uparrow d_\downarrow\rangle)/\sqrt{2} + 0.065(\lvert\phi^a_\uparrow\phi^s_\downarrow\rangle + \lvert\phi^a_\downarrow\phi^s_\uparrow\rangle)/\sqrt{2}$
−9.551860	$0.9\lvert d'_\downarrow d_\downarrow\rangle + 0.33\lvert\phi^s_\downarrow d'_\downarrow\rangle - 0.27\lvert\phi^a_\downarrow d_\downarrow\rangle + 0.065\lvert\phi^a_\downarrow\phi^s_\downarrow\rangle$
−8.395675	$0.7\lvert d_\uparrow d_\downarrow\rangle - 0.49(\lvert\phi^s_\downarrow d_\uparrow\rangle - \lvert\phi^s_\uparrow d_\downarrow\rangle)/\sqrt{2} - 0.45\lvert d'_\uparrow d'_\downarrow\rangle - 0.24(\lvert\phi^a_\uparrow d'_\downarrow\rangle - \lvert\phi^a_\downarrow d'_\uparrow\rangle)/\sqrt{2} + 0.092\lvert\phi^s_\uparrow\phi^s_\downarrow\rangle - 0.035\lvert\phi^a_\uparrow\phi^a_\downarrow\rangle$
−8.322127	$0.85(\lvert d'_\uparrow d_\downarrow\rangle - \lvert d'_\downarrow d_\uparrow\rangle)/\sqrt{2} - 0.41(\lvert\phi^s_\uparrow d'_\downarrow\rangle - \lvert\phi^s_\downarrow d'_\uparrow\rangle)/\sqrt{2} + 0.44(\lvert\phi^a_\downarrow d_\uparrow\rangle - \lvert\phi^a_\uparrow d_\downarrow\rangle)/\sqrt{2} - 0.088(\lvert\phi^a_\uparrow\phi^s_\uparrow\rangle - \lvert\phi^a_\downarrow\phi^s_\downarrow\rangle)/\sqrt{2}$
E (eV)	Three-hole eigenstate
−8.066426	$0.68\lvert d'_\uparrow(\lvert\phi^s_\downarrow d_\downarrow\rangle - \lvert\phi^s_\downarrow d_\uparrow d_\downarrow\rangle)/\sqrt{2} - 0.35\lvert d'_\uparrow d_\uparrow d_\downarrow\rangle - 0.31\lvert\phi^s_\uparrow\phi^s_\downarrow d'_\downarrow\rangle + 0.3(\lvert\phi^a_\uparrow d'_\downarrow\rangle - \lvert\phi^a_\downarrow d'_\uparrow\rangle)/\sqrt{2} + 0.27\lvert\phi^a_\uparrow d_\uparrow d_\downarrow\rangle + 0.17\lvert d_\uparrow\rangle(\lvert\phi^s_\uparrow d'_\downarrow\rangle - \lvert\phi^s_\downarrow d'_\uparrow\rangle)/\sqrt{2}$ + small terms
−8.066426	$0.68\lvert d'_\downarrow(\lvert\phi^s_\downarrow d_\downarrow\rangle - \lvert\phi^s_\downarrow d_\uparrow d_\downarrow\rangle)/\sqrt{2} - 0.35\lvert d'_\downarrow d_\uparrow d_\downarrow\rangle - 0.31\lvert\phi^s_\downarrow\phi^s_\uparrow d'_\downarrow\rangle + 0.3(\lvert\phi^a_\downarrow d'_\uparrow\rangle - \lvert\phi^a_\uparrow d'_\downarrow\rangle)/\sqrt{2} + 0.27\lvert\phi^a_\downarrow d_\uparrow d_\downarrow\rangle + 0.17\lvert d_\downarrow\rangle(\lvert\phi^s_\uparrow d'_\downarrow\rangle - \lvert\phi^s_\downarrow d'_\uparrow\rangle)/\sqrt{2}$ + small terms
−7.690491	$0.65\lvert d_\downarrow\rangle(\lvert\phi^a_\uparrow d'_\downarrow\rangle - \lvert\phi^a_\downarrow d'_\uparrow\rangle)/\sqrt{2} - 0.33\lvert d'_\uparrow d'_\downarrow d_\downarrow\rangle + 0.3\lvert\phi^s_\uparrow d'_\downarrow d_\downarrow\rangle - 0.26\lvert\phi^a_\uparrow\phi^a_\downarrow d_\downarrow\rangle - 0.31\lvert\phi^s_\downarrow\rangle(\lvert\phi^a_\uparrow d'_\downarrow\rangle - \lvert\phi^a_\downarrow d'_\uparrow\rangle)/\sqrt{2} + 0.21\lvert d'_\downarrow\rangle(\lvert\phi^a_\uparrow d_\downarrow\rangle - \lvert\phi^a_\downarrow d_\uparrow\rangle)/\sqrt{2}$ + small terms
−7.690491	$0.65\lvert d_\uparrow\rangle(\lvert\phi^a_\downarrow d'_\uparrow\rangle - \lvert\phi^a_\uparrow d'_\downarrow\rangle)/\sqrt{2} - 0.33\lvert d'_\downarrow d'_\uparrow d_\downarrow\rangle + 0.3\lvert\phi^s_\downarrow d'_\uparrow d_\downarrow\rangle - 0.26\lvert\phi^a_\downarrow\phi^a_\uparrow d_\downarrow\rangle - 0.31\lvert\phi^s_\uparrow\rangle(\lvert\phi^a_\downarrow d'_\uparrow\rangle - \lvert\phi^a_\uparrow d'_\downarrow\rangle)/\sqrt{2} + 0.21\lvert d'_\uparrow\rangle(\lvert\phi^a_\downarrow d_\downarrow\rangle - \lvert\phi^a_\uparrow d_\uparrow\rangle)/\sqrt{2}$ + small terms

TABLE II. Energy eigenvalues (in the first line) and the corresponding averaged hole numbers per orbitals for two small clusters. The second and the third columns correspond to a single Ni ion surrounded by six oxygen ions with three holes in total. The remaining columns correspond to the four-site square cluster with three Cu ions (orbitals d_1, ϕ_1^s, d_2, ϕ_2^s, d_3, ϕ_3^s), one Ni ion and six holes in total. In the latter case, the periodic boundary conditions have been employed. In both cases we set $\tilde{\Delta} = 1.4$ eV. The calculations involved repeated Lanczos diagonalization so that degeneracies could be resolved. The expectation values of the hole number operators corresponding to a particular energy eigenvalue were obtained by averaging over all the corresponding states.

Orb. \ E (eV)	−8.0664	−7.6905	−12.193	−12.035	−11.952	−11.874	−11.644	−11.563	−11.541	−11.42
d_0	1.09	0.793	0.995	0.875	0.985	0.876	0.936	0.986	0.981	0.851
d_0'	0.833	1.12	0.832	0.948	0.87	0.973	0.919	0.879	0.88	1.03
ϕ_0^s	0.902	0.214	0.473	0.231	0.489	0.407	0.382	0.409	0.352	0.362
ϕ_0^a	0.171	0.875	0.115	0.166	0.117	0.291	0.185	0.198	0.108	0.517
d_1	–	–	0.759	0.811	0.792	0.798	0.815	0.831	0.864	0.797
ϕ_1^s	–	–	0.363	0.526	0.323	0.441	0.398	0.394	0.374	0.312
d_2	–	–	0.759	0.811	0.792	0.798	0.815	0.831	0.864	0.797
ϕ_2^s	–	–	0.363	0.526	0.323	0.441	0.398	0.394	0.374	0.312
d_3	–	–	0.814	0.775	0.816	0.783	0.816	0.835	0.859	0.776
ϕ_3^s	–	–	0.527	0.332	0.493	0.191	0.336	0.243	0.344	0.246

triplet, singlet, and ZR doublet configurations of a Ni site are thus $-1/2K_{\mathrm{Ni}}$, $3/2K_{\mathrm{Ni}}$, and 0, respectively. We have further completely neglected the fifth term in Eq. (2), whose expectation values are small (see Fig. 1). We have also neglected the second and the third terms on the right-hand side of Eq. (4). The neglect of the second one is justified by small values of the magnitudes of the hopping parameters: the largest value of $|T'_{pd}\tau'^{s}_{i_0 j}|$ is approximately seven times smaller than that of $|T_{pd}\tau_{ij}|$. The neglect of the third term is consistent with that of the contributions of the A doublets on Ni. The effect of this term can be approximately captured by a lowering of the input energy of the Ni d' orbitals due to

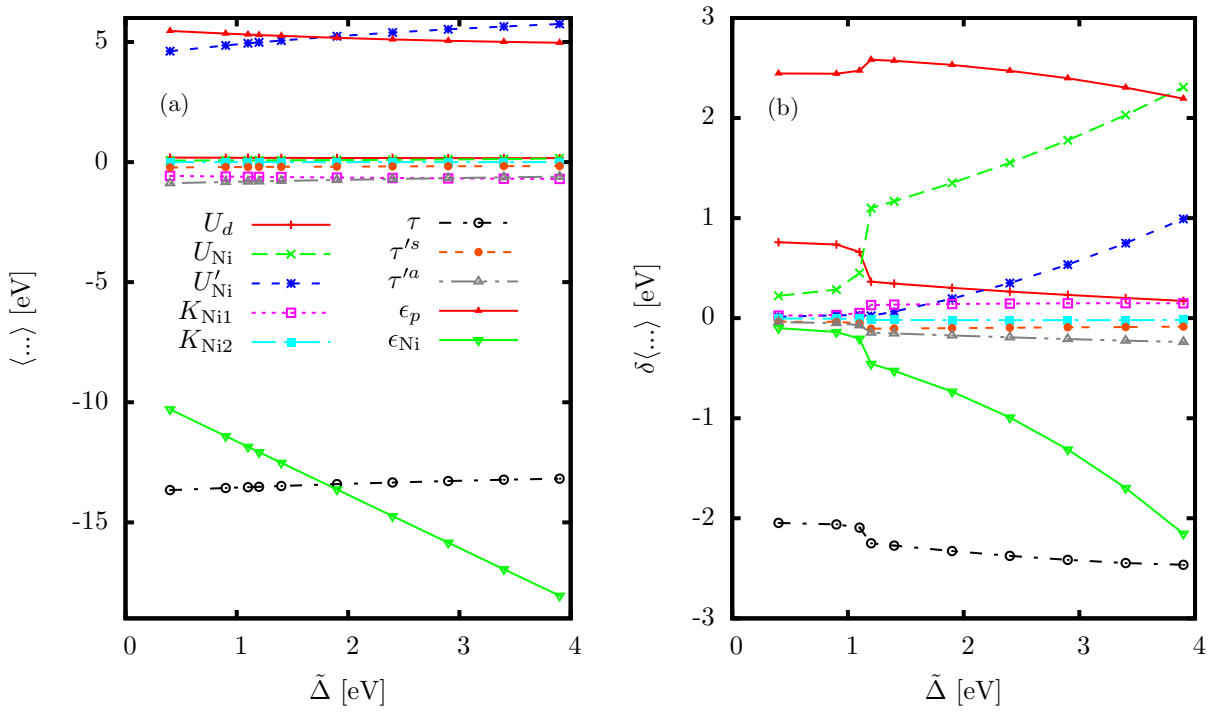

FIG. 1. (a) Expectation values of the components of the Hamiltonian given by Eqs. (2) and (4) as functions of the parameter $\tilde{\Delta} = \Delta_{\mathrm{Ni}} - \epsilon_p$ defined in the text for the undoped eight-site Hubbard cluster such as in Ref. [23] containing one Ni impurity, subject to the periodic boundary conditions. (b) Differences between the expectation values for the same cluster with one doped hole (i.e., ten holes in total) and those of the undoped case (nine holes in total). The steep changes around $\tilde{\Delta} = 1.2$ eV are due to the transition from a state with the doped hole in the Zhang-Rice singlet band to the state, where the hole occupies mainly the oxygen orbitals surrounding the Ni site, forming the Zhang-Rice doublet [23]. For an interpretation at the level of the effective model, see the discussion of Fig. 2.

the d'-ϕ^a hybridization. We have checked, however, that the impact of this correction is not important.

Based on the simplified Hamiltonian, we can now express the superexchange coupling constants and the effective hopping parameters. First, we address the superexchange. The magnetic interaction between two undoped Cu sites will be unaffected by the presence of Ni impurities since—up to the fourth order of perturbation theory—the corresponding expression involves only the two Cu sites and the oxygen p orbital connecting them. We thus have [28]

$$J = \frac{4T_{pd}^4}{\epsilon_p^3} + \frac{4T_{pd}^4}{\epsilon_p^2 U_d}. \tag{7}$$

For the coupling constant J_{NiCu} characterizing the interaction between the spin of the d orbital of a Ni site and that of a neighboring Cu site we similarly obtain

$$J_{\mathrm{NiCu}} = 2T_{pd}^4\left[\left(\frac{1}{\epsilon_p} + \frac{1}{\Delta_{\mathrm{Ni}}}\right)^2 \frac{1}{\epsilon_p + \Delta_{\mathrm{Ni}}} + \frac{1}{U_{\mathrm{Ni}} + K_{\mathrm{Ni}} - \tilde{\Delta}}\frac{1}{\epsilon_p^2} + \frac{1}{U_d + \tilde{\Delta}}\frac{1}{\Delta_{\mathrm{Ni}}^2}\right]. \tag{8}$$

For the values of the Hubbard model parameters presented in Ref. [23], the values of J and J_{NiCu} are similar. For the sake of simplicity, one common superexchange constant denoted as J will be used in the following.

For the hopping parameters characterizing the propagation of the ZR singlet/doublet we obtain, using the same type of perturbation approach as used by Zhang and Rice, the following formula:

$$t_{\mathbf{ij}} = -\frac{1}{2}\frac{T_{pd}^2}{U_d - \epsilon_p}\delta_{\langle \mathbf{i},\mathbf{j}\rangle} + 4\tau_{\mathbf{ij}}\lambda T_{pd}^2\left(\frac{1}{U_d - \epsilon_p} + \frac{1}{\epsilon_p}\right), \quad \mathbf{i},\mathbf{j} \neq \mathbf{i_0} \tag{9}$$

and

$$t_{\mathbf{i i_0}} = -\frac{1}{2}\frac{T_{pd}^2}{U_d - \epsilon_p}\delta_{\langle \mathbf{i},\mathbf{i_0}\rangle} + 2\tau_{\mathbf{i i_0}}\lambda T_{pd}^2\left(\frac{1}{U_d - \epsilon_p} + \frac{1}{\epsilon_p} + \frac{1}{U_{\mathrm{Ni}} - \Delta_{\mathrm{Ni}}} + \frac{1}{\Delta_{\mathrm{Ni}} - K_{\mathrm{Ni}}}\right), \tag{10}$$

where $\delta_{\langle \mathbf{i},\mathbf{j}\rangle} = 1$ for nearest neighbors and $=0$ otherwise and $\lambda = \frac{1}{N}\sum_{\mathbf{k}} \beta_{\mathbf{k}}^{-1} = 0.958$. The Cu-Cu hopping parameter given by Eq. (9) is unaffected by the presence of Ni impurities, the expression is the same as in Ref. [25]. The magnitude of the factor $\tau_{\mathbf{ij}}$ is the largest for nearest neighbors. With increasing distance, $|\tau_{\mathbf{ij}}|$ decreases fast. The Cu-Ni hopping parameter is given by Eq. (10). For the values of the Hubbard model parameters presented in Ref. [23], the numerical values of the two hopping parameters are very similar. For the sake of simplicity, one common nearest neighbor hopping constant denoted by t will be used in the following and couplings between more distant neighbors will be neglected.

With the expressions for the two parameters J and t, the construction of an ordinary t-J-like model would be complete. However, in the present lattices with Cu and Ni sites, an important role is also played by the difference between the binding energy of the ZR singlet and that of the ZR doublet (at the Ni sites). Within a t-J-like model, the latter can be represented by an additional component describing a change of energy of a hole upon entering a Ni d orbital. The complete t-J-like Hamiltonian for a Ni substituted CuO_2 plane containing this component (the third term with the parameter E_{Ni}) and the Hund's rule coupling term, reads

$$H_{tJ}^{\mathrm{Ni}} = t\sum_{\langle \mathbf{ij}\rangle\sigma}(\tilde{d}_{\mathbf{i}\sigma}^{\dagger}\tilde{d}_{\mathbf{j}\sigma} + \mathrm{H.c.}) + J\sum_{\langle \mathbf{ij}\rangle}\left(\mathbf{S_i}\mathbf{S_j} - \frac{1}{4}n_{\mathbf{i}}n_{\mathbf{j}}\right) + E_{\mathrm{Ni}}\sum_{\mathbf{i_0}} n_{\mathbf{i_0}} - 2K_{\mathrm{Ni}}\sum_{\mathbf{i_0}}\mathbf{S}'_{\mathbf{i_0}}\mathbf{S}_{\mathbf{i_0}}, \tag{11}$$

where $\tilde{d}$ is the projected fermion operator $\tilde{d}_{\mathbf{j}\sigma} = d_{\mathbf{j}\sigma}(1 - n_{\mathbf{j},-\sigma})$. In the numerical calculations we use the following values of J and K_{Ni}: $J = 0.3t$ and $K_{\mathrm{Ni}} = 2.3t$. The former is common in the physics of cuprates, the latter is consistent with the value of K_{Ni} of Ref. [23] of 0.8 eV and the value of t of 0.35 eV that we obtain from Eq. (9). It remains to find a suitable value for the parameter E_{Ni}. For this purpose we have used the similarity between the role of E_{Ni} within the effective model and that of $\varepsilon_{\mathrm{Ni}}$ within the Hubbard model. As mentioned above, for the Hubbard model there is a critical value of $\tilde{\Delta}$ $(= -\varepsilon_{\mathrm{Ni}} - U_{\mathrm{Ni}} + 3K_{\mathrm{Ni}})$ of $\sim$1.2 eV, at which the averaged number $\langle n(\mathrm{Ni})\rangle$ of holes at the Ni site jumps to higher values, see Fig. 1(b) of Ref. [23]. Figure 2 shows that the E_{Ni} dependence of $\langle n(\mathrm{N}i)\rangle$ from the effective model based calculation is fairly similar to the $\varepsilon_{\mathrm{Ni}}$ dependence in the Hubbard case. The fact that the onset of $\langle n(\mathrm{N}i)\rangle$ is much steeper for the 16-site cluster than for the other two clusters, is likely due to the specific symmetry of the former. Note that for low values of E_{Ni} (e.g., for $E_{\mathrm{Ni}} = -2$ eV) the values of $\langle n(\mathrm{Ni})\rangle$ for the three clusters are close to each other. At the level of the effective model, the jump of $\langle n(\mathrm{N}i)\rangle$ can be interpreted in

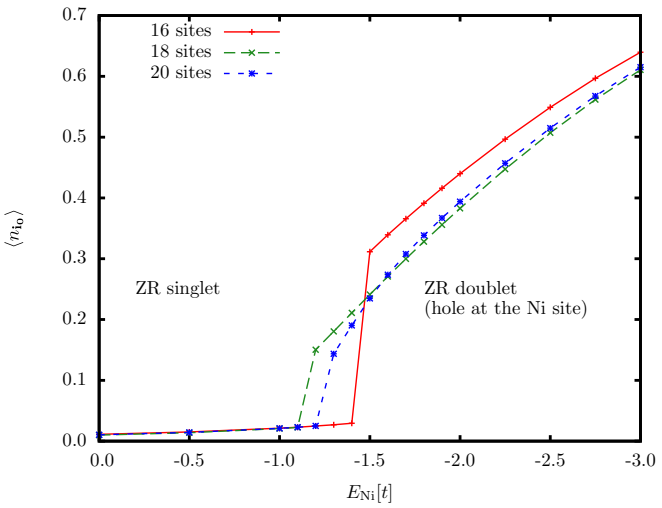

FIG. 2. Averaged number of holes at the Ni site as a function of the energy E_{Ni} defined in the text, calculated using the effective Hamiltonian of Eq. (11), for several clusters containing one hole and one impurity.

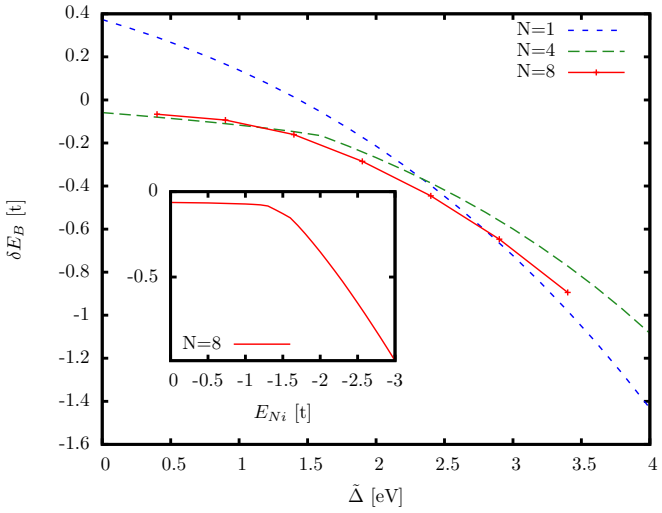

FIG. 3. Binding energy difference δE_{B} defined by Eq. (12) obtained by exact diagonalization of the Hubbard Hamiltonian given by Eqs. (2) and (4), as a function of the quantity $\tilde{\Delta}$ defined in the text, for three small Hubbard clusters. Clusters with four and eight sites were studied using the periodic boundary condition, the single site cluster with the open boundary condition. Inset: δE_{B} obtained using the effective Hamiltonian given by Eq. (11), as a function of E_{Ni}, for the eight-site cluster.

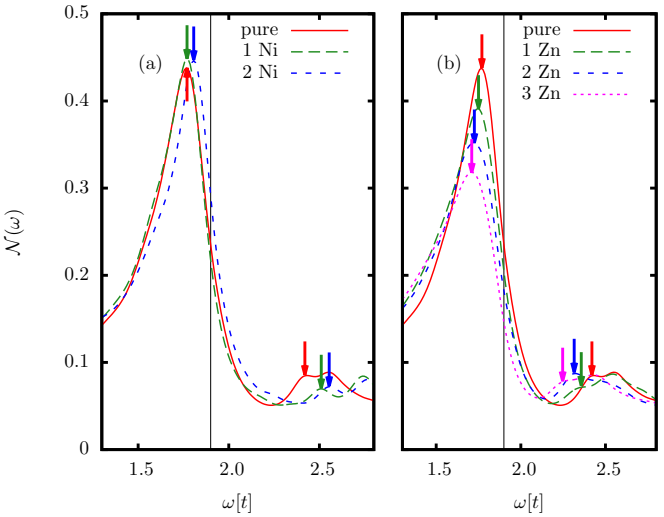

FIG. 4. Densities of states for clusters of 26 sites and one hole. (a) The solid red line corresponds to the pure case and the dashed green/short dashed blue line to the case with one/two Ni impurities/26 sites. (b) The solid red line has the same meaning as in (a). The long dashed/short dashed/dotted lines correspond to 1/2/3 Zn impurities/26 sites. The arrows indicate the energies of the limits of the pseudogap as described in the text. The vertical lines indicate the position of the chemical potential for the pure case.

simple terms: It occurs at an energy close to $-K_{\mathrm{Ni}}/2$, the value of the on-site Hund's rule exchange for the triplet states. For higher values of E_{Ni}, the triplet configuration is more stable than the ZR doublet and the doped hole prefers the Cu sites. For lower values of E_{Ni}, the situation is the reverse, and the hole prefers to reside in the ZR doublet at the Ni site. The similarity between the role of E_{Ni} within the effective model and that of $\varepsilon_{\mathrm{Ni}}$ within the Hubbard model can also be seen in the trends of the binding energy difference δE_B defined by

$$\delta E_B = E^1_{\text{GS-Ni}} - E^0_{\text{GS-Ni}} - \left(E^1_{\text{GS-Cu}} - E^0_{\text{GS-Cu}}\right), \tag{12}$$

where $E^0_{\text{GS-Ni}}$ ($E^1_{\text{GS-Ni}}$) is the ground state energy of the undoped (doped with one hole) cluster with one Ni impurity, and $E^0_{\text{GS-Cu}}$ ($E^1_{\text{GS-Cu}}$) is the ground state energy of the undoped (doped with one hole) cluster without Ni impurities. Figure 3 shows the $\tilde{\Delta}$ dependence of δE_B for three small Hubbard clusters and, in the inset, the E_{Ni} dependence of δE_B for the eight-site effective model cluster. It can be seen that the dependencies are qualitatively very similar. Tsutsui *et al.* used, in most of their calculations, a value of $\varepsilon_{\mathrm{Ni}}$ by $\sim$0.2 eV lower than the critical one (i.e., $\tilde{\Delta} = 1.4$ eV, $\sim$0.2 eV higher than the threshold value), assuming that the Ni impurities bind the doped holes. Following their considerations we have chosen, in most of our calculations, the value of E_{Ni} of $-2t$, few tenths of eV lower than the threshold. It can be seen in Fig. 3 that the corresponding value of δE_B of approximately $-0.4t$ would be obtained within the Hubbard model for $\tilde{\Delta} \approx 2.0$ eV.

Concerning the Zn substituted case, we have adopted the simple model proposed in Ref. [22], where the Zn sites participate neither in hopping nor in superexchange. The Hamiltonian reads

$$H^{\mathrm{Zn}}_{tJ} = t \sum_{\langle \mathbf{ij}\rangle\sigma,\mathbf{i},\mathbf{j}\neq\mathbf{i_0}} (\tilde{d}^\dagger_{\mathbf{i}\sigma}\tilde{d}_{\mathbf{j}\sigma} + \mathrm{H.c.}) + J \sum_{\langle \mathbf{ij}\rangle\mathbf{i},\mathbf{j}\neq\mathbf{i_0}} \left(\mathbf{S_i}\mathbf{S_j} - \frac{1}{4}n_i n_{\mathbf{j}}\right), \tag{13}$$

where i_0 denotes the Zn sites.

III. RESULTS AND DISCUSSION

A. Many body density of states

Here we present results of our calculations of the many body density of states $\mathcal{N}$ defined by

$$\mathcal{N}(\omega) = 2/N \sum_{\mathbf{k}} A(\mathbf{k},\omega), \tag{14}$$

where $A(\mathbf{k},\omega)$ is the quasiparticle spectral function

$$A(\mathbf{k},\omega) = -(1/\pi)\mathrm{Im}G(\mathbf{k},\omega) \tag{15}$$

and $G(\mathbf{k},\omega)$ is the retarded Green's function

$$G(\mathbf{k},\omega) = -i \int_0^\infty dt e^{i\omega t} \langle\{\tilde{d}_{\mathbf{k}\sigma}(t), \tilde{d}^\dagger_{\mathbf{k}\sigma}(0)\}\rangle. \tag{16}$$

The many body density of states $\mathcal{N}(\omega)$ can be equivalently expressed as a (site) averaged local density of states.

Our main results are contained in Figs. 4, 5, 6, and 8. They were obtained by numerical diagonalization of the standard t-J Hamiltonian (for the pure CuO_2 plane), of the effective Hamiltonian of Eq. (11) (for the Ni substituted CuO_2 plane) and of the effective Hamiltonian of Eq. (13) (for the Zn substituted CuO_2 plane). We have used the following values of the input

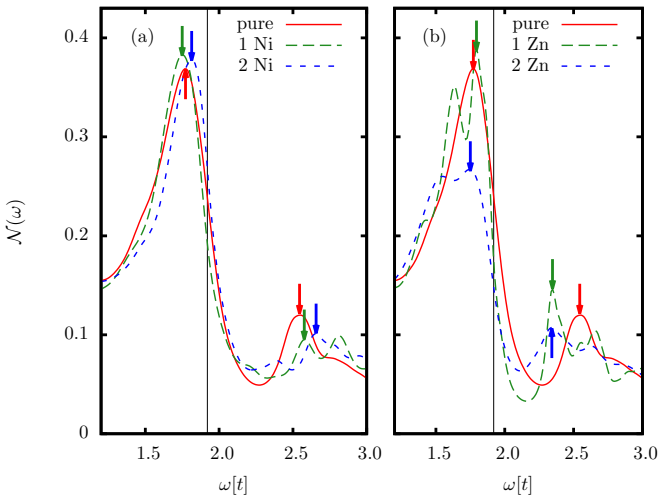

FIG. 5. Densities of states for clusters of 20 sites and one hole. (a) The solid red line corresponds to the pure case and the green long dashed (blue short dashed) line to the case with one (two) Ni impurities/20 sites. (b) The solid red line has the same meaning as in (a). The green long dashed/blue short dashed lines correspond to the case with one (two) Zn impurities/20 sites. The arrows indicate the energies of the limits of the pseudogap as described in the text. The vertical lines indicate the position of the chemical potential for the pure case.

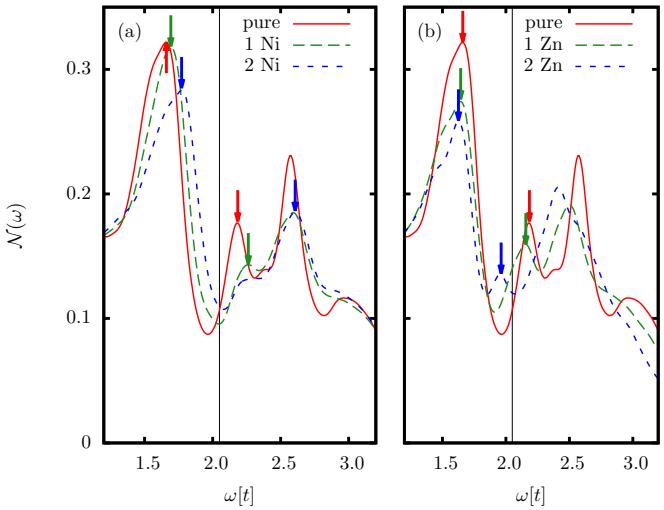

FIG. 6. Densities of states for clusters of 20 sites and two holes. (a) The solid red line corresponds to the pure case and the green long dashed (blue short dashed) line to the case with one (two) Ni impurities/20 sites. (b) The solid red line has the same meaning as in (a). The green long dashed/blue short dashed lines correspond to the case with one (two) Zn impurities/20 sites. The arrows indicate the energies of the limits of the pseudogap as described in the text. The vertical lines indicate the position of the chemical potential for the pure case. In the case of two Ni impurities, there is an ambiguity in the location of the arrow at the electron side of μ. We have decided to attach the arrow to the main maximum rather than to the shoulder feature located closer to μ.

parameters: $J = 0.3t$, $K_{\mathrm{Ni}} = 2.3t$, and $E_{\mathrm{Ni}} = -2t$. The δ peaks in the expression for $A(\mathbf{k},\omega)$ were replaced with Lorentzians, $\delta(\omega - \omega') \to 1/\pi \times \gamma/[\gamma^2 + (\omega - \omega')^2]$ with $\gamma = 0.1t$.

Figures 4 and 5 show the many body densities of states (densities of states in the following) for clusters of 26 sites and one hole and 20 sites and one hole, respectively. The vertical lines indicate the position of the chemical potential μ determined by

$$\int_{-\infty}^{\infty} d\omega \mathcal{N}(\omega) f(\omega - \mu) = 1 - \delta, \tag{17}$$

for the pure case. Here f stands for the Fermi Dirac function and δ is the concentration of holes, here $\delta = 1/N$. For the Ni and Zn substituted cases the positions of the chemical potential are similar. It can be seen that all the spectra exhibit a depletion of $\mathcal{N}(\omega)$ slightly above the chemical potential. Figure 6 shows the spectra of $\mathcal{N}(\omega)$ for clusters of 20 sites and two holes. Again, a depletion of the density of states near the chemical potential can be seen. This feature was first noticed, for the pure case, by Prelovšek and co-workers [18–20] and associated with the pseudogap phenomenon occurring in underdoped cuprates. These authors have further shown that with increasing temperature μ moves towards the minimum of $\mathcal{N}(\omega)$. The present figures highlight the sensitivity of the pseudogap to the presence of Ni and Zn impurities. It can be seen that the width of the pseudogap decreases (increases) with Zn doping (Ni doping).

In order to compare different configurations and also to compare with experimental data, a method to estimate the width of the pseudogap is needed. For the present purposes we have defined the width of the pseudogap Ω_{PG} as $\Delta_e - \Delta_h$, where Δ_e is the energy of the first maximum at the right-hand side of μ or—in the absence of a sharp maximum—the energy of the shoulder feature at the low energy side of a broad complex maximum, and Δ_h is the energy of the pronounced maximum at the left-hand side of μ. In the figures the energies are denoted by the arrows. The origin of the structures is illustrated in Fig. 7 showing the hole and electron components of the quasiparticle spectral function $A(\mathbf{k},\omega)$ for the cluster of 26 sites and one hole (for the pure case). The vertical solid red line indicates the energy difference $E_{\mathrm{GS}}(C_{26,1,0}) - E_{\mathrm{GS}}(C_{26,2,0})$, where E_{GS} stands for the ground state energy and $C_{N,M,P}$ for the cluster with N sites, M holes, and P impurities. The vertical dashed green line indicates the energy difference $E_{\mathrm{GS}}(C_{26,0,0}) - E_{\mathrm{GS}}(C_{26,1,0})$. Note that the ground states of $C_{26,0,0}$ and $C_{26,2,0}$ are singlets with the total quasimomentum [0,0], the ground state of $C_{26,1,0}$ is a doublet with the total quasimomentum $\in \{[\pm 4\pi/13, \pm 6\pi/13]\}$. For other one hole doped clusters, the ground state quasimomenta are also close or equal to $[\pm\pi/2, \pm\pi/2]$. The finite distance between the two vertical lines is partially caused by the fact that the ground state of $C_{26,2,0}$ is a bound state of two holes. It can be seen in the figure how the maximum of $\mathcal{N}(\omega)$ at Δ_h arises. The maximum of $\mathcal{N}(\omega)$ at Δ_e can be seen to arise from the contributions of several $\mathbf{k}$ points to the electron component of $\mathcal{N}(\omega)$. The energy Δ_e can be expressed as $E_m(C_{26,0,0}) - E_{\mathrm{GS}}(C_{26,1,0})$, where $E_m(C_{26,0,0})$ is a characteristic energy of the underlying states of the undoped cluster $C_{26,0,0}$. It can be further seen that the width of the pseudogap Ω_{PG} can be approximated by the distance in energy between the vertical dashed green

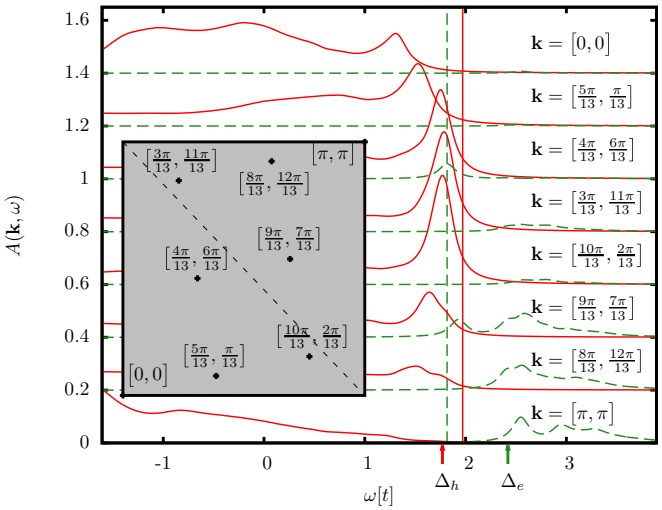

FIG. 7. Hole (solid red lines) and electron (dashed green lines) components of the quasiparticle spectral function $A(\mathbf{k},\omega)$ for the cluster of 26 sites, one hole, and no impurities. The vertical solid red line indicates the energy difference $E_{GS}(C_{26,1,0}) - E_{GS}(C_{26,2,0})$, and the vertical dashed green line indicates the energy difference $E_{GS}(C_{26,0,0}) - E_{GS}(C_{26,1,0})$. The meaning of the energies Δ_h and Δ_e is described in the text. The inset shows the positions of the $\mathbf{k}$ vectors in the first quadrant of the Brillouin zone.

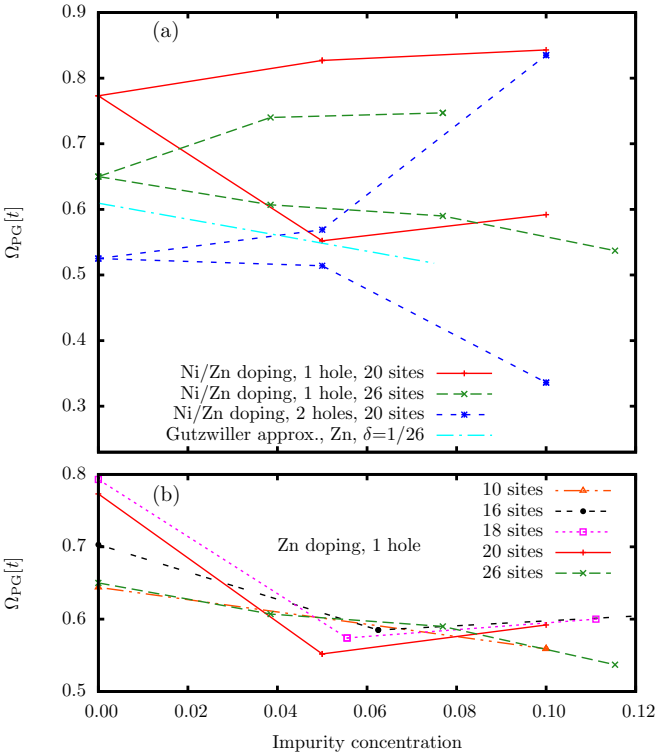

FIG. 8. (a) Magnitude of the pseudogap Ω_{PG} deduced from the calculated spectra of the density of states as a function of Ni/Zn concentration for three selected clusters. The upper branch always corresponds to the Ni doping, the lower one to the Zn doping. The cyan dot dashed line displays the result obtained by using the RVB mean field approach as described in the text. (b) The Zn concentration dependencies of Ω_{PG} for $N = 10$, 16, 18, 20, and 26, and one doped hole.

line and Δ_e that is equal to $E_m(C_{26,0,0}) - E_{GS}(C_{26,0,0})$, a characteristic excitation energy of the parent antiferromagnet. Physically, the present pseudogap is caused simply by the fact that for a vast majority of states created by the "filling in the hole" the antiferromagnetic order—in a real doped system a short range fluctuating antiferromagnetic/RVB order—is considerably damaged, i.e., a high energy spin excitation is present.

Figure 8(a) shows Ω_{PG} as a function of Ni/Zn concentration (δ_{Ni}/δ_{Zn}) for three selected clusters. For each size of the cluster and for each hole doping the upper branch corresponds to the Ni case and the bottom branch to the Zn case. Figure 8(b) shows the δ_{Zn} dependencies of Ω_{PG} for $N = 10$, 16, 18, 20, and 26, and one doped hole. The locations of the impurities are shown in the Appendix. In the pure, one-hole case, Ω_{PG} is only weakly size dependent. This confirms that the present pseudogap is not an artifact resulting from finite size effects. The magnitude of the pseudopap Ω_{PG} decreases when δ_{Zn} increases from 0 to $1/N$. Let us focus on the one-hole case. It can be seen in (b) that the magnitude of the decrease is relatively small for $N = 10$ and $N = 26$ and large for $N = 18$ and $N = 20$, $N = 16$ is intermediate between the two groups. When going from $\delta_{Zn} = 1/N$ to $\delta_{Zn} = 2/N$, Ω_{PG} decreases further for $N = 26$ and very slightly increases in the other cases. In all cases, however, the magnitude of the decrease of Ω_{PG} when going from $\delta_{Zn} = 0$ to $\delta_{Zn} \approx 0.1$ is in the range from $0.1t$ to $0.2t$, confirming that the Zn doping induced suppression of the pseudogap is not an artifact resulting from finite size effects. In most cases, Ω_{PG} decreases with increasing Ni concentration. Exceptions are the cases of 20 sites and one hole and 26 sites and one hole where Ω_{PG} hardly changes upon increasing the impurity concentration from $1/N$ to $2/N$.

The decrease of Ω_{PG} with increasing Zn concentration can be interpreted in terms of the RVB mean field approach developed by Zhang, Gros, Rice, and Shiba [29–31]. The mean field Hamiltonian for the pure case reads

$$H = g_t t \left(\sum_{\langle \mathbf{ij} \rangle \sigma} d^{\dagger}_{\mathbf{i}\sigma} d_{\mathbf{j}\sigma} + \text{H.c.} \right) + g_s J \sum_{\langle \mathbf{ij} \rangle} \mathbf{S_i S_j}, \qquad (18)$$

where $g_t = 2\delta/(1+\delta)$ and $g_s = 4/(1+\delta)^2$ are the Gutzwiller renormalization factors. The magnitude of the pseudogap to be compared with Ω_{PG} from exact diagonalization is given by $2\Delta_{PG}$, where Δ_{PG} is the amplitude of the superconducting gap of d-wave symmetry, resulting from the standard variational approach to the problem given by the Hamiltonian (18). The latter amplitude can be expressed as $(3/4)g_S J\overline{\Delta}$, where $\overline{\Delta}$ is the dimensionless amplitude [29]. For the limit of $\delta = 0$, we obtain $2\Delta_{PG} = 6J\overline{\Delta}(\delta = 0)$ and—using the calculated value of $\overline{\Delta}(\delta = 0)$ of ~0.33—further $2\Delta_{PG} \approx 2J$. With increasing δ, $2\Delta_{PG}$ decreases. Note that the values of Ω_{PG} for the pure case shown in Fig. 6 are fairly close to $2J$ (i.e., $0.6t$) and that there is a decrease of Ω_{PG} with increasing doping (when going from $C_{20,1,0}$ to $C_{20,2,0}$). Consider now the Zn doped case. Within the model given by the Hamiltonian (13), the nearest neighbor links involving a Zn site participate neither in hopping nor

in superexchange. As a consequence, the number of nearest neighbor links available for hopping and superexchange is reduced by a factor of $(1-2\delta_{\rm Zn})$ with respect to the pure case. This leads to a reduction of the Gutzwiller renormalization factors $g_t \to (1-2\delta_{\rm Zn})g_t$ and $g_s \to (1-2\delta_{\rm Zn})g_s$, and to the corresponding reduction of the magnitude of the pseudogap $2\Delta_{\rm PG} \to (1-2\delta_{\rm Zn})2\Delta_{\rm PG}$. The cyan dot dashed line in Fig. 8 displays the $\delta_{\rm Zn}$ dependence of $2\Delta_{\rm PG}$ calculated in this way for $\delta = 1/26$. It can be seen that the slope of the $\delta_{\rm Zn}$ dependence is very close to that resulting from exact diagonalization for the largest cluster.

Next we demonstrate that the increase of $\Omega_{\rm PG}$ with increasing Ni concentration $\delta_{\rm Ni}$ is due to the binding of holes to the Ni sites discussed in Sec. II, captured by the $E_{\rm Ni}$ term of the effective Hamiltonian (11). We begin with considerations of the density of states of clusters of the type $C_{N,1,1}$ (one hole, one Ni impurity). We have (i) $E_m(C_{N,0,1}) \approx E_m(C_{N,0,0})$, because the effect of one Ni impurity in the undoped case is not very pronounced; (ii) $E_{\rm GS}(C_{N,1,1}) < E_{\rm GS}(C_{N,1,0})$, because of the binding of the hole to the impurity; and (iii) approximately the same value of Δ_h as in the pure case, because the bound state around the Ni impurity is not available for the second hole. As a consequence, we obtain $\Delta_e(C_{N,1,1}) > \Delta_e(C_{N,1,0})$ and $\Omega_{\rm PG}(C_{N,1,1}) > \Omega_{\rm PG}(C_{N,1,0})$. This explains the corresponding trend in Fig. 8. Next we consider clusters of the type $C_{N,1,2}$ containing two Ni impurities. Using similar arguments as above, we obtain $\Omega_{\rm PG}(C_{N,1,2}) \approx \Omega_{\rm PG}(C_{N,1,1})$, in agreement with the results for $C_{26,1,1}$ and $C_{26,1,2}$, and $C_{20,1,1}$ and $C_{20,1,2}$ shown in Fig. 8. Consider further clusters of the type $C_{N,2,0}$, $C_{N,2,1}$, and $C_{N,2,2}$. First, when going from $C_{N,2,0}$ to $C_{N,2,1}$, $\Omega_{\rm PG}$ can be expected to increase, because one of the holes gets bound to the impurity and only one mobile hole remains, the system becoming effectively less doped. This accounts for a slight increase of $\Omega_{\rm PG}$ when going from $C_{20,2,0}$ to $C_{20,2,1}$ shown in Fig. 8. Second, when going from $C_{N,2,1}$ to $C_{N,2,2}$, both holes get bound to the impurities and $\Omega_{\rm PG}$ can be expected to approach the result for $C_{N,1,1}$. This is consistent with the results for $C_{20,2,2}$ and $C_{20,1,1}$ shown in Fig. 8. The correlation between $\Omega_{\rm PG}$ and the hole binding to the impurity [described by the $E_{\rm Ni}$ term in Eq. (11)] manifests itself in the dependence of the many body density of states on the parameter $E_{\rm Ni}$, specifying the strength of the binding, shown in Fig. 9. It can be clearly seen that $\Omega_{\rm PG}$ increases with decreasing $E_{\rm Ni}$. This is further analyzed in Fig. 10 demonstrating that the enhancement of the pseudogap by a Ni impurity is largely determined by the Ni site terms of the Hamiltonian (11).

Based on our results for small clusters we can offer some speculations on the $\delta_{\rm Ni}$ dependence of $\Omega_{\rm PG}$ in the limit of $N \to \infty$. For $\delta_{\rm Ni} \geqslant \delta$ most of the holes can be expected to be at least weakly bound to the impurities and $\Omega_{\rm PG}$ to be larger than $\Omega_{\rm PG}(\delta \to 0, \delta_{\rm Ni} = 0)$ by a fraction of the binding energy, similarly as in the cases of one hole and one impurity and two holes and two impurities addressed above. For $\delta_{\rm Ni} \leqslant \delta$, only some of the doped holes can be expected to be bound, the remaining ones mobile, the corresponding fractions being $\approx \delta_{\rm Ni}$ and $\approx \delta - \delta_{\rm Ni}$, respectively. The decrease of the fraction of mobile holes from δ to $\approx \delta - \delta_{\rm Ni}$ upon Ni doping can be expected to cause an increase of $\Omega_{\rm PG}$ similar to the one that would occur in the absence of impurities as a consequence of the decrease of δ by $\delta_{\rm Ni}$.

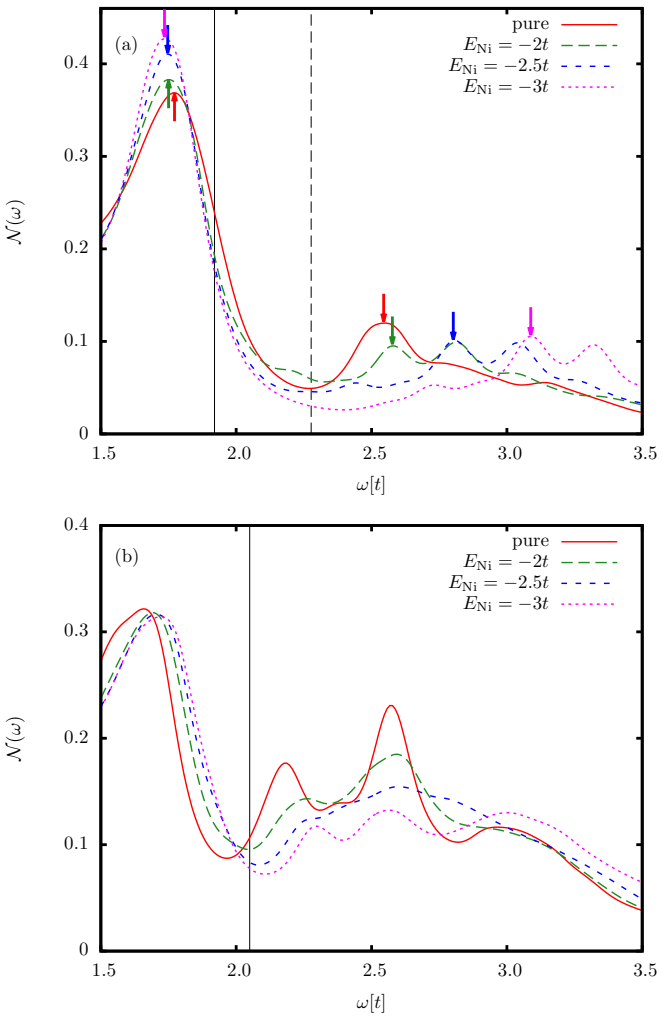

FIG. 9. Densities of states for clusters of 20 sites and one Ni impurity, for several values of the parameter $E_{\rm Ni}$ specifying the hole energy at the impurity site. (a) and (b) The one hole and the two hole cases, respectively. The arrows in (a) indicate the energies of the limits of the pseudogap as described in the text. The solid vertical lines indicate the positions of the chemical potential for the pure cases, calculated using Eq. (17). The dashed vertical line in (a) indicates the position of the chemical potential used in the calculation providing the long dashed green line in Fig. 11.

B. *c*-axis conductivity

The pseudogap occurring in the density of states manifests itself also in the spectra of the real part σ_{1c} of the c-axis conductivity [18]. In order to explore the effect of the Ni substitution, we have calculated σ_{1c} using Eq. (4) from Ref. [18],

$$\sigma_c(\omega) \sim \frac{1}{\omega}\int d\omega' [f(\omega'-\mu) - f(\omega'+\omega-\mu)] \times \mathcal{N}(\omega')\mathcal{N}(\omega'+\omega) \qquad (19)$$

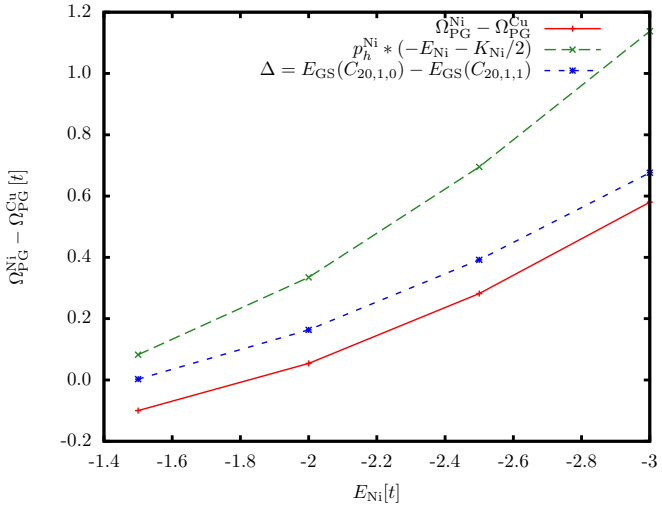

FIG. 10. Impact of the hole binding to the impurity on the width of the pseudogap Ω_{PG}. The solid red line represents the enhancement of the pseudogap by a Ni impurity $\Omega_{PG}^{Ni} - \Omega_{PG}^{Cu}$ as a function of the hole energy E_{Ni} at the Ni site, for the cluster of 20 sites and one hole. Here Ω_{PG}^{Ni} (Ω_{PG}^{Cu}) is the width of the pseudogap for the Ni substituted (pure) case. The values of Ω_{PG}^{Ni} and Ω_{PG}^{Cu} have been obtained as distances between the arrows in Fig. 9. The long dashed green line represents the contribution of the Ni sites, i.e., of the third and the fourth terms on the right-hand side of Eq. (11), to the difference $\Delta = E_{GS}(C_{20,1,0}) - E_{GS}(C_{20,1,1})$. It is given by $p_h^{Ni}(-E_{Ni} - K_{Ni}/2)$, where p_h^{Ni} is the probability that the doped hole is located at the Ni site. Finally, the short dashed blue line shows the E_{Ni} dependence of Δ.

that is well justified in the limit of weak interlayer coupling, and the calculated spectral functions, for the pure case and for the case with one Ni impurity. The chemical potential μ has been fixed by the standard condition (17). Results of our calculations are shown in Fig. 11. It can be seen that the

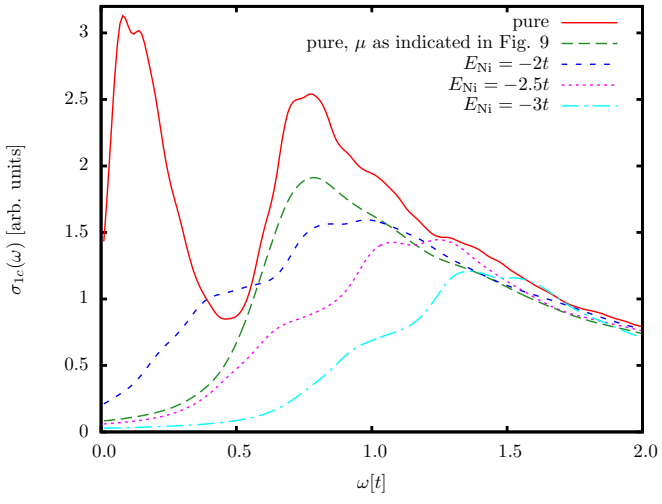

FIG. 11. Spectra of the real part of the c-axis conductivity calculated for clusters with 20 sites and one doped hole. The solid red line and the long dashed green line correspond to the pure case. The latter represents the result of the calculation with the chemical potential specified in Fig. 9. The other lines correspond to the cases with one Ni impurity.

density of states pseudogap of magnitude Ω_{PG} gives rise to a dip feature in the spectra of $\sigma_{1c}(\omega)$ with an onset at about Ω_{PG}. For $\omega < \Omega_{PG}$, $\sigma_{1c}(\omega)$ is lower that what one would obtain by a simple extrapolation from high frequencies, where $\sigma_{1c}(\omega)$ is a decreasing function. In the following, we denote this feature as the c-axis conductivity pseudogap. In the case of one Ni impurity and $E_{Ni} = -2t$, the width of the c-axis conductivity pseudogap, i.e., the energy of the onset of the dip, is slightly larger than that of the pure case, in agreement with the trend established for the density of states pseudogap. It can be further seen that the width increases with increasing binding energy of the hole to the impurity, in agreement with the trend illustrated in Fig. 9. The maximum at low energies occurring in the spectra for the pure case (solid red line) is, as we believe, an artifact due to finite size effects or due to a pair formation occurring at low temperatures. It is absent in the spectrum calculated with the chemical potential located at the energy of the minimum of $\mathcal{N}(\omega)$, that is represented by the long dashed green line.

Next we compare our results with the experimental data of Ref. [16]. We begin with the pseudogap in the pure, one hole case. Its width amounts to 0.6–0.8t, for a typical value of t of 0.4 eV, we obtain 0.24–0.32 eV. This is well comparable to the low doping limit of the experimental value of Ω_{PG} of ∼260 meV. There is a qualitative difference between the shape of the calculated spectra and that of the experimental low temperature data of $YBa_2Cu_3O_{7-\delta}$: in the experimental spectra the conductivity increases slightly as a function of frequency even above the pseudogap energy. This difference is likely due to the influence of the intrabilayer component of the conductivity that gives rise to the transverse plasma mode [32–39] and has a strong impact on the electronic background. At the model level, the presence of a Ni impurity leads to a slight enhancement of the pseudogap. Unfortunately, Ref. [16] does not contain data of strongly underdoped Ni substituted samples to be compared with our results. Based on the data points in Fig. 2(c) of Ref. [16], however, it can be speculated that the low doping limit of the width of the pseudogap increases only slightly with Ni substitution (from ∼260 to ∼300 meV), in agreement with our observations. We cannot reproduce the experimentally observed dramatic increase of the pseudogap width upon Ni substitution in moderately underdoped samples (Fig. 1(f) of Ref. [16]), but it can be qualitatively understood in terms of a Ni induced reduction of the fraction of mobile holes discussed in the last paragraph of Sec. III A.

IV. SUMMARY AND CONCLUSIONS

We performed exact diagonalization calculations for effective t-J-like models representing the CuO_2 plane where some of the Cu ions are replaced with Zn/Ni in order to clarify the trends occurring in the c-axis infrared conductivity (σ_c) data of Zn and Ni substituted (Sm,Nd)$Ba_2Cu_3O_{7-\delta}$ crystals reported by Pimenov and co-workers. The effective Hamiltonian for the Ni substituted case has been obtained by a sequence of approximations from a more complete model involving Cu $3d$, Ni $3d$, and O $2p$ orbitals, proposed as a starting point for analyzing the role of Ni impurities by Tsutsui and co-workers. The calculated spectra of the many body density of states and of the real part of σ_c display the pseudogap discovered by Prelovšek and co-workers. We show that its width Ω_{PG}

decreases with increasing Zn concentration, in agreement with Pimenov's data. The decrease can be qualitatively understood in terms of a suppression of short range spin correlations, and approximately reproduced by the RVB mean field approach. Concerning the Ni case, we have found that the energy Ω_{PG} increases—for realistic values of the parameters characterizing the impurity—with Ni doping, again in agreement with Pimenov's data. For clusters with one doped hole, the increase upon adding a Ni impurity is clearly due to the binding of the hole to the Ni site, addressed within the more complete model by Tsutsui and co-workers, and to the fact that the impurity does not cause a pronounced suppression of spin correlations. Based on this finding and further results for 1–2 holes and 1–2 Ni impurities, we suggest that in the real Ni substituted CuO_2 plane the concentration of mobile holes is approximately equal to $\max\{0,\delta-\delta_{\mathrm{Ni}}\}$, where δ and δ_{Ni} are the hole and Ni concentrations, respectively. The energy Ω_{PG} can therefore be expected to be larger than for the pure CuO_2 plane due to the binding of the doped holes to the Ni sites and effective underdoping. Our results support the point of view that the pseudogap is caused by strong spin correlations. In the present study we have limited ourselves to investigations of the pseudogap. Future exact diagonalization studies addressing the impacts of Zn and Ni impurities on the hole-hole correlation function (e.g., along the lines of Refs. [40,41]) might help to clarify the observed differences between the influences of Zn and Ni on superconductivity in the high-T_c cuprates [42–44].

ACKNOWLEDGMENTS

A part of the work was carried out under the project CEITEC - Central European Institute of Technology that was supported by the European Regional Development Fund, Project No. CZ.1.05/1.1.00/02.0068. The work was also supported by the projects MUNI/A/1496/2014 and MUNI/A/1388/2015. Computational resources were provided by the MetaCentrum under the program LM2010005 and the CERIT-SC under the program Centre CERIT Scientific Cloud, part of the Operational Program Research and Development for Innovations, Reg. No. CZ.1.05/3.2.00/08.0144. Discussions with C. Bernhard and J. Chaloupka are gratefully acknowledged. We thank K. Tsutsui for communications concerning the results reported in Ref. [23] and H. Růžičková, P. Karlubíková, and J. Chaloupka for critical reading of the manuscript.

APPENDIX

Locations of the impurities are shown in Fig. 12.

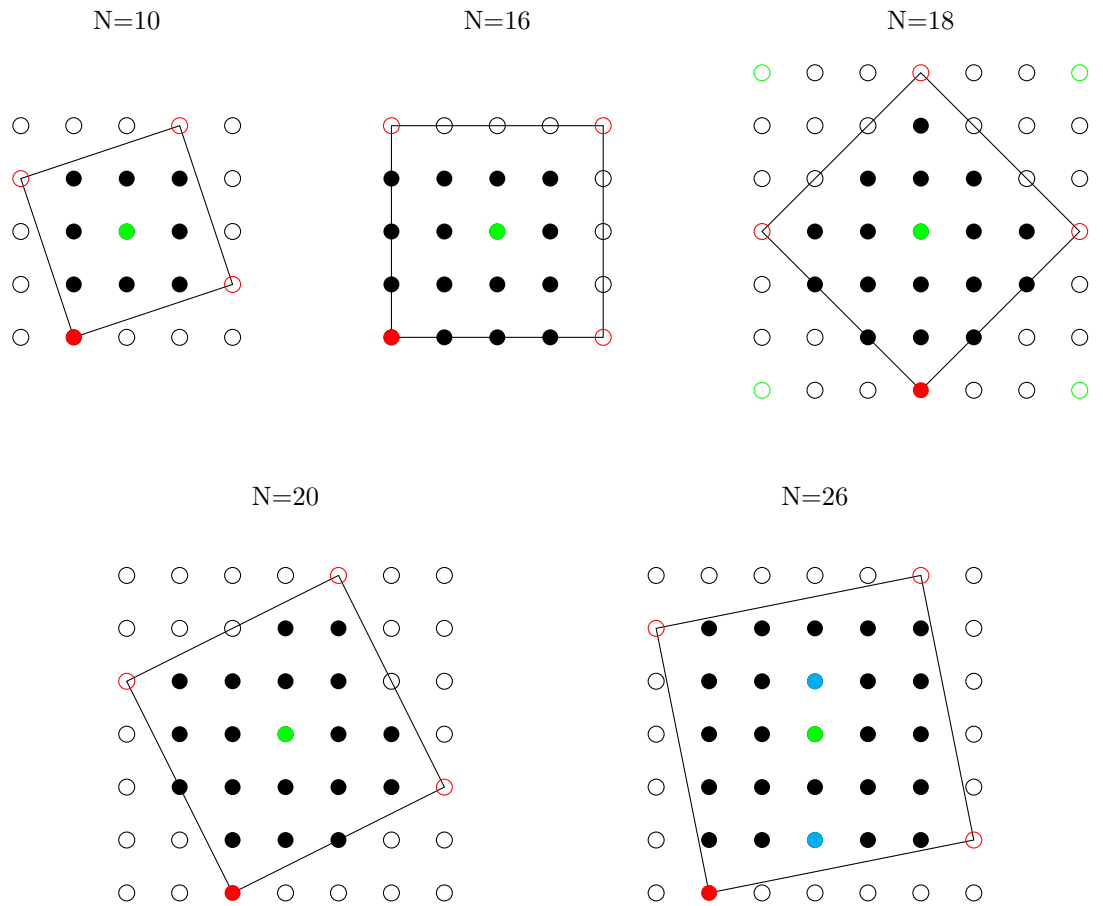

FIG. 12. Schematic representation of the clusters used in our calculations. In the calculations with two impurities (three impurities, $N = 26$ only), the latter were situated at the sites denoted by the red and the green circles (by the red and the blue circles). The sites are selected so as to maximize the interimpurity distances.

[1] W. W. Warren, R. E. Walstedt, G. F. Brennert, R. J. Cava, R. Tycko, R. F. Bell, and G. Dabbagh, Phys. Rev. Lett. **62**, 1193 (1989).

[2] H. Alloul, T. Ohno, and P. Mendels, Phys. Rev. Lett. **63**, 1700 (1989).

[3] C. C. Homes, T. Timusk, R. Liang, D. A. Bonn, and W. N. Hardy, Phys. Rev. Lett. **71**, 1645 (1993).

[4] D. S. Marshall, D. S. Dessau, A. G. Loeser, C. H. Park, A. Y. Matsuura, J. N. Eckstein, I. Bozovic, P. Fournier, A. Kapitulnik, W. E. Spicer, and Z. X. Shen, Phys. Rev. Lett. **76**, 4841 (1996).

[5] V. M. Krasnov, A. Yurgens, D. Winkler, P. Delsing, and T. Claeson, Phys. Rev. Lett. **84**, 5860 (2000).

[6] V. M. Krasnov, Phys. Rev. B **91**, 224508 (2015).

[7] For a review see T. Timusk and B. Statt, Rep. Prog. Phys. **62**, 61 (1999).

[8] For a review see M. R. Norman, D. Pines, and C. Kallin, Adv. Phys. **54**, 715 (2005).

[9] For a review see M. Hashimoto, I. M. Vishik, R.-H. He, T. Devereaux, and Z. X. Shen, Nat. Phys. **10**, 483 (2014).

[10] For a review see B. Keimer, S. A. Kivelson, M. R. Norman, S. Uchida, and J. Zaanen, Nature (London) **518**, 179 (2015).

[11] T. Timusk, Solid State Commun. **127**, 337 (2003).

[12] C. Bernhard, D. Munzar, A. Wittlin, W. König, A. Golnik, C. T. Lin, M. Kläser, Th. Wolf, G. Müller-Vogt, and M. Cardona, Phys. Rev. B **59**, R6631 (1999).

[13] L. Yu, D. Munzar, A. V. Boris, P. Yordanov, J. Chaloupka, Th. Wolf, C. T. Lin, B. Keimer, and C. Bernhard, Phys. Rev. Lett. **100**, 177004 (2008).

[14] A. Dubroka, M. Rössle, K. W. Kim, V. K. Malik, D. Munzar, D. N. Basov, A. A. Schafgans, S. J. Moon, C. T. Lin, D. Haug, V. Hinkov, B. Keimer, Th. Wolf, J. G. Storey, J. L. Tallon, and C. Bernhard, Phys. Rev. Lett. **106**, 047006 (2011).

[15] E. Uykur, K. Tanaka, T. Masui, S. Miyasaka, and S. Tajima, Phys. Rev. Lett. **112**, 127003 (2014).

[16] A. V. Pimenov, A. V. Boris, Li Yu, V. Hinkov, Th. Wolf, J. L. Tallon, B. Keimer, and C. Bernhard, Phys. Rev. Lett. **94**, 227003 (2005).

[17] For a review see J. Spalek, Acta Phys. Polon. A **111**, 409 (2007).

[18] P. Prelovšek, A. Ramšak, and I. Sega, Phys. Rev. Lett. **81**, 3745 (1998).

[19] P. Prelovšek, J. Jaklič, and K. Bedell, Phys. Rev. B **60**, 40 (1999).

[20] J. Jaklič and P. Prelovšek, Adv. Phys. **49**, 1 (2000).

[21] N. Lin, E. Gull, and A. J. Millis, Phys. Rev. B **82**, 045104 (2010).

[22] D. Poilblanc, D. J. Scalapino, and W. Hanke, Phys. Rev. Lett. **72**, 884 (1994).

[23] K. Tsutsui, A. Toyama, T. Tohyama, and S. Maekawa, Phys. Rev. B **80**, 224519 (2009).

[24] K. Ishii, K. Tsutsui, K. Ikeuchi, I. Jarrige, J. Mizuki, H. Hiraka, K. Yamada, T. Tohyama, S. Maekawa, Y. Endoh, H. Ishii, and Y. Q. Cai, Phys. Rev. B **85**, 104509 (2012).

[25] F. C. Zhang and T. M. Rice, Phys. Rev. B **37**, 3759 (1988).

[26] A. M. Oleś, Phys. Rev. B **28**, 327 (1983).

[27] For an effective Hamiltonian describing these processes see T. Xiang, Y. H. Su, C. Panagopoulos, Z. B. Su, and L. Yu, Phys. Rev. B **66**, 174504 (2002).

[28] P. W. Anderson, Phys. Rev. **115**, 2 (1959).

[29] F. C. Zhang, C. Gros, T. M. Rice, and H. Shiba, Supercond. Sci. Technol. **1**, 36 (1988).

[30] For a review, see P. W. Anderson, P. A. Lee, M. Randeira, T. M. Rice, N. Trivedi, and F. C. Zhang, J. Phys.: Condens. Matter **16**, R755 (2004).

[31] For a review see B. Edegger, V. N. Muthukumar, and C. Gros, Adv. Phys. **56**, 927 (2007).

[32] D. van der Marel and A. Tsvetkov, Czech J. Phys. **46**, 3165 (1996).

[33] M. Grüninger, D. van der Marel, A. A. Tsvetkov, and A. Erb, Phys. Rev. Lett. **84**, 1575 (2000).

[34] D. Munzar, C. Bernhard, A. Golnik, J. Humlíček, and M. Cardona, Solid State Commun. **112**, 365 (1999).

[35] V. Železný, S. Tajima, D. Munzar, T. Motohashi, J. Shimoyama, and K. Kishio, Phys. Rev. B **63**, 060502 (2001).

[36] A. Dubroka and D. Munzar, Physica C **405**, 133 (2004).

[37] N. Shah and A. J. Millis, Phys. Rev. B **65**, 024506 (2001).

[38] J. Chaloupka, C. Bernhard, and D. Munzar, Phys. Rev. B **79**, 184513 (2009).

[39] J. Vašátko and D. Munzar, Phys. Rev. B **86**, 014512 (2012).

[40] A. L. Chernyshev, P. W. Leung, and R. J. Gooding, Phys. Rev. B **58**, 13594 (1998).

[41] P. W. Leung, Phys. Rev. B **73**, 014502 (2006).

[42] S. H. Pan, E. W. Hudson, K. M. Lang, H. Eisaki, S. Uchida, and J. C. Davis, Nature (London) **403**, 746 (2000).

[43] E. W. Hudson, K. M. Lang, V. Madhavan, S. H. Pan, H. Eisaki, S. Uchida, and J. C. Davis, Nature (London) **411**, 920 (2001).

[44] For a review see H. Alloul, J. Bobroff, M. Gabay, and P. J. Hirschfeld, Rev. Mod. Phys. **81**, 45 (2009).